


Article

Influences of Anthropogenic Pollution on the Dynamics of Sedimentary Fulvic Acid Fractions as Revealed via Spectroscopic Techniques Combined with Two-Dimensional Correlation Spectroscopy

Yanchun Xiao ¹, Huibin Yu ^{2,*} and Yonghui Song ^{2,*} 

¹ Institute of Agricultural Engineering Technology, Fujian Academy of Agricultural Sciences, Fuzhou 350003, China; FAASHJKXGroup@163.com

² Watershed Research Center for Comprehensive Treatment of Water Environmental Pollution, Chinese Research Academy of Environmental Sciences, Beijing 100012, China

* Correspondence: yhbybx@163.com (H.Y.); songyh@craes.org.cn (Y.S.)

Abstract: To identify the influences of anthropogenic activities on the composition, spatial distribution, sources, and transformation mechanism of sedimentary fulvic acid (FA) fractions from different reaches of an urban river were tracked via excitation-emission matrix (EEM) fluorescence spectroscopy with parallel factor (PARAFAC) analysis and two-dimensional correlation spectroscopy (2D-COS). Sediment samples were collected from Baitapu River (BR) along gradients with human activities (e.g., rural, town, and urban sections) in Shenyang, northeast China, from which FA fractions were extracted and then determined via EEM fluorescence spectroscopy. According to optical indices, the autochthonous sources of sedimentary FA fractions in BR were more significant than the terrestrial sources. Among the sections, the contribution from autochthonous sources decreased in the following order: Rural > Urban > Town. Six components of sedimentary FA fractions were identified via EEM-PARAFAC: C1 comprised tryptophan-like (TRL) compounds; C2 was associated with microbial humic-like (MHL) compounds; C3, C4, and C5 were associated with FA-like (FAL) compounds; and C6 comprised humic acid-like (HAL) compounds. The proportion of sedimentary FA fractions decreased in the following order: MHL + FAL + HAL (humus, 77.37–88.90%) > TRL (protein, 11.10–22.63%) for the three sections, showing that humus dominated. The town section exhibited the highest sedimentary FA fractions (5328.87 ± 1315.82 Raman unit [R.U.]), followed by the urban (4146.49 ± 535.75 R.U.) and rural (2510.56 ± 611.00 R.U.) sections. Three pollution sources were determined via principal component analysis (i.e., the dominant industrial source, domestic wastewater, and agricultural effluent). Additionally, the results from 2D-COS revealed that sedimentary FA fractions tended to stabilize as the protein-like component was transformed into the HAL component. Furthermore, we used the structural equation model to validate the critical environmental variables affecting the FA fraction transformation. The results can elucidate the influences of human activities on the dynamics of sedimentary FA fractions in urban rivers.

Keywords: river sediment; fulvic acid fractions; variation; parallel factor analysis; structural equation model



Citation: Xiao, Y.; Yu, H.; Song, Y. Influences of Anthropogenic Pollution on the Dynamics of Sedimentary Fulvic Acid Fractions as Revealed via Spectroscopic Techniques Combined with Two-Dimensional Correlation Spectroscopy. *Water* **2023**, *15*, 2256. <https://doi.org/10.3390/w15122256>

Academic Editor: Luisa Bergamin

Received: 22 May 2023

Revised: 12 June 2023

Accepted: 14 June 2023

Published: 16 June 2023



Copyright: © 2023 by the authors. Licensee MDPI, Basel, Switzerland. This article is an open access article distributed under the terms and conditions of the Creative Commons Attribution (CC BY) license (<https://creativecommons.org/licenses/by/4.0/>).

1. Introduction

River sediments are an important part of the river ecosystem and function as the main carriers and significant heterogeneous adsorbents for migrating, transforming, and accumulating environmental pollutants [1,2]. Thus, they can significantly influence the water quality and ecological functions of river ecosystems [3,4]. Fulvic acid (FA) fractions are black substances enriched in sediments, which present a strong adsorption capacity with contaminants [5,6]. Previous studies have reported that sedimentary FA fractions play

an important role in governing the environmental geochemistry behavior of heavy metal pollutants, which is attributed to the active functional groups such as phenolic, carboxyl, and nitrogen-containing groups [7,8]. Nevertheless, few studies have been conducted on the dynamics of sedimentary FA fractions. The external input of sedimentary FA fractions is mainly influenced by anthropogenic activities (e.g., agriculture practices, industrialization, and urbanization) [9]. They usually show spatial variations, and the dynamics of the fractions are closely linked to environmental variables [10,11]. Therefore, it is necessary to further elucidate the effects of environmental variables and transformation mechanisms of sedimentary FA fractions, which is crucial for managing urban rivers.

The interactive mechanism of FA fractions and fluorophore groups can be described via excitation–emission matrix (EEM) fluorescence spectroscopy [12]. Furthermore, parallel factor (PARAFAC) analysis can mathematically decompose an EEM spectrogram into individual fluorescent components and quantify its relative content by weakening the interference from overlapping fluorophores [13,14]. Two-dimensional correlation spectroscopy (2D-COS) proved an effective technique in spectrum analysis, and it was generally used to improve the resolution of spectra, establish unambiguous assignments, and determine the sequence of the spectra [15]. Cui et al. [7] identified three components from the FA EEM, each component with two ligands, and assessed the interaction of different FA ligands and heavy metals via EEM-PARAFAC and 2D-COS combined technology; that is, high humification FA ligand with more metal-binding sites had the strong metal-binding ability and low metal-binding speed, whereas, low humification FA ligand presented high metal-binding speed. Structural equation models (SEM) can be used to identify underlying processes or unmeasured “latent” variables and explore the theoretical and empirical relationships of variables in a network form [16]. In this study, we employed EEM-PARAFAC, 2D-COS, and SEM to reveal the dynamic changes and transformation mechanisms of sedimentary FA fractions affected by multiple anthropogenic activities.

Considering the unique geological features of the Baitapu River (BR) in Shenyang, northeastern China, and the related human activities, we investigated the effects of anthropogenic activities on the transformation of sedimentary FA fractions. Numerous farmlands, industrial parks, and residential communities exist along the banks of BR, which can be divided into different ecosystem compartments (i.e., rural, town, and urban sections). Thus, it is ideal for studying the dynamic changes in sedimentary FA fractions derived from different anthropogenic activities. In recent years, sewage emission caused by increased agricultural activities, industrial manufacturing, and population has deteriorated water quality [17]. Moreover, the Chinese Environmental Quality Standards for Surface Water (GB-3838-2002) has classified the water environment of BR to be below grade V, which necessitates urgent treatment. Consequently, identifying pollution sources and tracking the variation of sedimentary FA fractions to facilitate pollution control is vital. The main objectives of this study are: (1) to investigate the occurrence and spatial distributions of sedimentary FA fractions in different ecosystem compartments of BR; (2) to identify potentially anthropogenic pollution sources of sedimentary FA fractions through combined statistical analysis models; (3) to compare the variations in FA fractions in different ecosystem compartments and establish the differences and similarities; and (4) to explore the potential mechanisms of transformation of sedimentary FA fractions from urban rivers, which is important to reveal the fate of sedimentary FA fractions in aquatic systems. The results can provide a theoretical basis and support for preventing anthropogenic pollutants in urban rivers.

2. Materials and Methods

2.1. Sampling and Processing

BR (41°37′–41°43′ N, 123°39′–123°20′ E) is a level-one tributary of the Hunhe River in Shenyang, Liaoning, China, with a total length of 51.5 km and a basin area of 182 km². BR belongs to a continental semi-humid climate zone with a mean annual average precipitation of 600 to 800 mm and a mean annual average temperature of 6.2 °C to 9.7 °C. It comprises

the central area of Shenyang City, including Hunnan District and Heping District, and flows from southeast to northwest through different geological units (Figure 1). The runoff is associated with agriculture; livestock and poultry breeding; and industrial, domestic, and natural activities. In addition, its annual mean runoff volume is 227.2 million m³/year, which is its main source of water supply [17]. Owing to the low flow rate in BR, which plays a vital role in pollutant retention, BR is divided into three ecosystem compartments: agricultural, industrial, and urban.

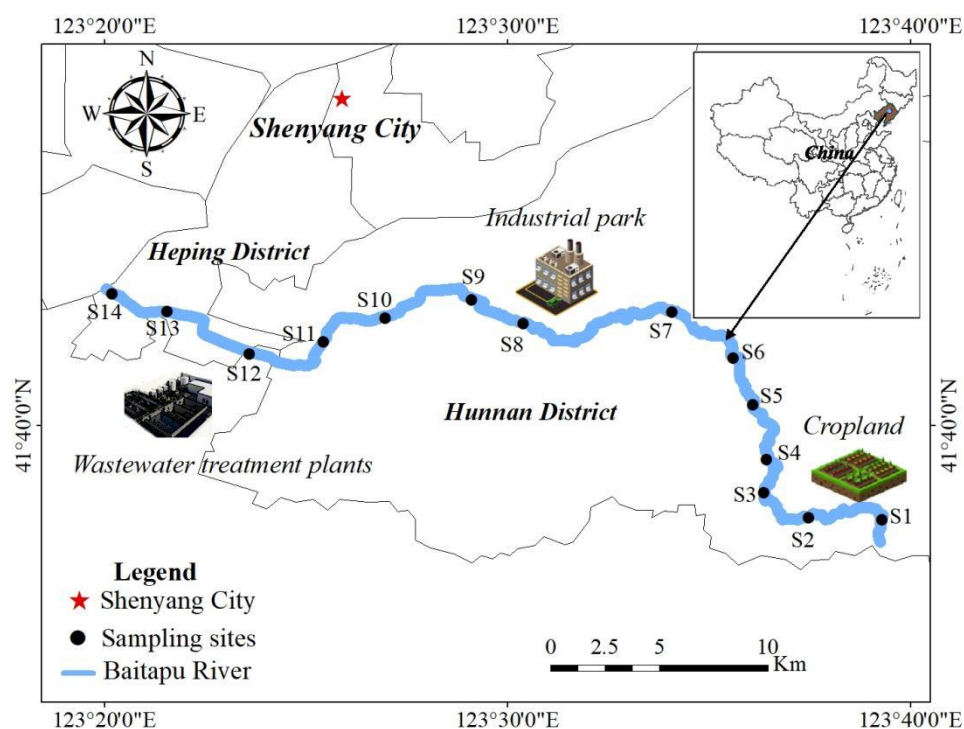


Figure 1. Distribution of sediment samples from BR taken in April 2016.

To cover the three major ecosystem compartments, potential pollution sources, and hydraulic characteristics, 14 sampling sites along BR were selected (Figure 1). Among them, sites S1 to S4 are located in the upper reach covering the rural region, where rural domestic sewage, effluent from livestock and poultry farms, and agriculture sewage are discharged. S5 to S8 is situated in the middle reach covering the town region, where industrial wastewater and domestic sewage are discharged through sewage pipes. S9 to S14 are located in the lower reach covering the urban region, which is affected by effluent from wastewater treatment plants. In April 2016, surface sediments of 0–10 cm were collected using a Peterson grab sampler (ETC200, Shanghai, China). To avoid potential bias caused by accidental sampling, five surface sediments (~1.0 kg) were collected from the center point of the sampling site and four positive directions toward the east, west, south, and north according to the BR section width. Seventy sediment samples were collected from these sites and refrigerated for transport to the laboratory within 12 h of sampling. All sediment samples were freeze-dried, crushed, and sieved through a 0.2 mm mesh sieve before analysis.

2.2. Sedimentary FA Fraction Extraction

Sedimentary FA fraction extraction was performed following the International Humic Substances Society (IHSS) recommendations. In short, 10-g freeze-dried, crushed, and sieved sediment was suspended in 100-mL mixed solution (50 mL of 0.1 M Na₄P₂O₇·10H₂O and 50 mL of 0.1 M NaOH) to maintain the dry sediment to liquid ratio at 1:10. Subsequently, the suspension was shaken for 24 h (200 rpm) at 25 °C in the absence of light. The supernatant was collected by settling the sediment after centrifugation at 8500 rpm for

10 min. This process was repeated in triplicate, and the supernatant was pooled together to filter through a 0.45- μm Millipore membrane to obtain a humus solution. Then, 6 M HCl was added into the humus solution to adjust the pH value to 1–2, and the supernatant was collected after precipitation at 4 °C for 12 h to obtain the FA fractions.

2.3. Physicochemical Analysis

The pH and electrical conductivity (EC) of the sediment were determined in a sediment/water suspension (sediment/water ratio = 1:2.5) using a multifunctional water analyzer (Hydrolab DS5, HACH, USA). The DO concentration of overlying bottom water (5 ± 1 cm above the sediment) was recorded at the time of sampling in the field using the Hydrolab DS5 water analyzer. The total nitrogen (TN) content of the sediment was measured with a continuous-flow automated analyzer (FUTURA, Alliance, France) after digestion with $\text{H}_2\text{SO}_4\text{-H}_2\text{O}_2$ [18]. The total phosphorus (TP) content of the sediment was analyzed using the Murphy-Riley method after digestion with $\text{H}_2\text{SO}_4\text{-HClO}_4$ [19]. The combustion oxidation nondispersive infrared absorption method (HJ 501-2009) was used to measure the total organic carbon (TOC) content of sedimentary FA fractions with a TOC analyzer (TOC-LCPH, Shimadzu, Japan).

2.4. Fluorescence Measurements and PARAFAC Analysis

The fluorescence EEM spectra of sedimentary FA fractions were obtained using a fluorescence spectrometer (Hitachi F-7000, Tokyo, Japan). Wavelengths of the excitation (E_x) and emission (E_m) were at 200–450 (step 5 nm) and 260–550 (step 5 nm), respectively, with a scan rate of $2400 \text{ nm}\cdot\text{min}^{-1}$ [20]. Each measured EEM was corrected for the inner-filter effect according to the absorption spectra of the same sample, and the blank signals of Milli-Q water were subtracted to eliminate the influence of Raman scattering. Rayleigh scattering was eliminated using an interpolation technique. The Rayleigh scattering and spectrum data of the upper side were set to zero to eliminate the Rayleigh scattering effect [21]. Then, the corrected EEM was modeled with PARAFAC using MATLAB R2019a software with the DOMFluor toolbox (www.models.life.ku.dk, version 1.7) [22]. The correct number of identified fluorescent components was determined via residual analysis, split-half analysis, and visual inspection. Fluorescence intensity was normalized to Raman units (R.U.), and the relative concentrations of each component were estimated using maximum fluorescence intensity (F_{max}). The contribution of each component to the total fluorescence (%C1–%C6) was used as indices for the composition of sedimentary FA fractions.

Three optical indices, namely, fluorescence index (FI), biological index (BIX), and humification index (HIX) were used to infer the aromaticity, source, and humification degree of sedimentary FA fractions, respectively, which could be calculated using EEM data [23]. Higher (>1.9) and lower (<1.4) values of FI indicate weak and strong aromaticity, respectively [24]. Higher BIX (>1) and HIX (>10) are associated with a stronger biological/aquatic bacterial contribution and a higher humic content. In comparison, lower BIX (<0.8) and HIX (<4) are associated with a weaker contribution from autochthonous sources and a lower humification degree [25]. The three indices are calculated and interpreted using the following formulas:

$$FI = \frac{I_{370/450}}{I_{370/500}}, \quad (1)$$

$$BIX = \frac{I_{310/380}}{I_{310/430}}, \quad (2)$$

$$HIX = \frac{\sum I_{254/435 \rightarrow 480}}{\sum I_{254/300 \rightarrow 345}}, \quad (3)$$

where I indicates the fluorescence intensity at each specific E_x/E_m wavelength pair or range.

2.5. Two-Dimensional Correlation Spectroscopy (2D-COS) Analysis

Two-dimensional COS analysis using 2D Shige software version 1.3 (Kwansei-Gakuin University, XiGong, Japan) can provide specific orders of component variation information under external perturbations. The variation in sedimentary FA fractions can be investigated via 2D-COS analysis according to the E_x loadings of the PARAFAC components [26]. Noda et al. [27] summarized the rules for analyzing synchronous and asynchronous maps. If the signs of the two maps are the same in a given wavelength range, the event at the x-coordinate is precedent to that at the y-axis, while if the signs are opposite, the preferential changes are reversed with respect to the coordinates [28].

2.6. Statistical Analysis

Principal component analysis (PCA) is an excellent statistical tool for handling multivariate data with minimum loss of information [29]. PCA was performed to identify the possible sources and compositions of sedimentary FA fractions from BR using pH, EC, DO, TN, TP, TOC, FI, BIX, HIX, and the F_{\max} of C1–C6.

Path analysis based on a structural equation model (SEM) was used to predict interactive relationships between observed and latent variables and causality among latent variables [30]. The applicability and overall goodness-of-fit test for SEM were determined using the ratio of Chi-square, degrees of freedom, and significance coefficient (i.e., Chi-square/df is less than 5, and the p -value is less than 0.05) [31].

3. Results and Discussion

3.1. Physicochemical Parameters

The three sections exhibited variations in physicochemical parameters (Table S1 and Figure S1). The average pH of the sediments gradually increased from the rural (7.62 ± 0.28) to town (7.85 ± 0.35) sections, and the pH of the urban section (6.77 ± 0.69) was significantly lower than those of the rural and town sections. Zhang et al. [12] reported that the relative abundance of *Anaerolineae* in sediment from the urban section was higher than those in sediments from the rural and town sections, which facilitated protein degradation, accompanied by the production of a large amount of organic acid, resulting in a weakly acidic environment in the sediment from the urban section. The urban section exhibited the highest mean EC value ($511.50 \pm 330.95 \mu\text{S}\cdot\text{cm}^{-1}$), followed by the rural ($400.44 \pm 58.87 \mu\text{S}\cdot\text{cm}^{-1}$) and town ($357.47 \pm 98.34 \mu\text{S}\cdot\text{cm}^{-1}$) sections, consistent with the results of Mahabeer et al. [32]. The urban dominant zones exhibited the highest EC value, and agricultural activities increased the EC value through the enrichment of pollutants from the associated anthropogenic activities. The DO concentration of the overlying bottom water from BR varied significantly from 0.15 to $1.67 \text{ mg}\cdot\text{L}^{-1}$, which was lower than the monitoring threshold ($\text{DO} < 2 \text{ mg}\cdot\text{L}^{-1}$) according to the guidelines for the treatment of rural black and black-odorous water (trial) (China 2019). This indicates that the sediments in the whole river were all in a hypoxic state [33].

Additionally, the average content of TN increased from the rural ($2283.33 \pm 880.83 \text{ mg}\cdot\text{kg}^{-1}$) to town ($3176.80 \pm 547.94 \text{ mg}\cdot\text{kg}^{-1}$) sections and then decreased in the urban ($2554.68 \pm 1089.90 \text{ mg}\cdot\text{kg}^{-1}$) section. The town section exhibited the highest TN, which may be related to the industrial activities in this region. A large fertilizer factory, identified in the industrial park along the town section, was possibly one of the leading contributors to the elevated TN level in this section. The average TN content in the rural section was comparable to that in the urban section, which may be related to non-point sources from the predominant farming across the rural region, where nitrogen-containing fertilizers could be leached into BR owing to surface runoff. Furthermore, the mean TP content in the rural ($842.22 \pm 436.98 \text{ mg}\cdot\text{kg}^{-1}$) section was approximately half of those in the town ($1777.62 \pm 643.39 \text{ mg}\cdot\text{kg}^{-1}$) and urban ($1870.12 \pm 1086.19 \text{ mg}\cdot\text{kg}^{-1}$) sections. Phosphorous is relatively immobile in soils, and given its application as fertilizer in farming activities in rural areas, phosphorus uptake by biota increases its retention in the area [32]. In contrast, in the town and urban areas, phosphorus could enter the

river system through impervious structures in the anthropogenic zones. According to the sediment pollution evaluation criteria proposed by the United States Environmental Protection Agency (EPA), over 90% of the 14 sampling sites were heavily contaminated ($TN > 2000 \text{ mg}\cdot\text{kg}^{-1}$, $TP > 600 \text{ mg}\cdot\text{kg}^{-1}$), indicating that river ecosystems were destroyed by human activities, leading to eutrophication. Moreover, the average TOC content of sedimentary FA fractions decreased in the following order: Town ($65.18 \pm 31.36 \text{ mg}\cdot\text{L}^{-1}$) > Urban ($30.98 \pm 13.20 \text{ mg}\cdot\text{L}^{-1}$) > Rural ($20.57 \pm 6.38 \text{ mg}\cdot\text{L}^{-1}$), which showed that the town section exhibited the highest TOC, related to the industrial and residential activities. The effluent from the industrial park with $20,000 \text{ m}^3\cdot\text{days}^{-1}$ entered into the river at site S8; consequently, it exhibited a higher TOC content than the other sampling sites. Specifically, the TOC content significantly varied throughout the sedimentary FA fractions, with a coefficient of variation (CV) of 69.38% (Table S1), indicating that the distributions of sedimentary FA fractions were strongly affected by multiple anthropogenic inputs and that significant spatial differences occurred.

3.2. Fluorescence Spectroscopy Characteristics of Sedimentary FA Fractions

Through visual inspection, three representative pollution source types were obtained in sedimentary FA fractions with six fluorescence peaks (Figure S2): peak tryptophan-like (TRL, $E_x/E_m = 225\text{--}237 \text{ nm}/340\text{--}381 \text{ nm}$); peak microbial humic-like (MHL, $E_x/E_m = 290\text{--}310 \text{ nm}/370\text{--}410 \text{ nm}$); peak soil-derived FA-like (FAL₁, $E_x/E_m = 260\text{--}300 \text{ nm}/400\text{--}500 \text{ nm}$); peak ultraviolet FA-like (FAL₂, $E_x/E_m = 237\text{--}260 \text{ nm}/400\text{--}500 \text{ nm}$); peak visible FA-like (FAL₃, $E_x/E_m = 300\text{--}370 \text{ nm}/400\text{--}500 \text{ nm}$); and peak terrestrial humic acid-like (HAL, $E_x/E_m = 370\text{--}390 \text{ nm}/480\text{--}500 \text{ nm}$) [20]. Sediments affected by different pollution sources were measured and plotted as an EEM spectrum with various advantageous peaks. In the spectrum of the sediments affected by agricultural effluent, peak FAL₂ was the predominant fluorophore of FA fractions (Figure S2a). The sedimentary FA fractions dominated by peak MHL, FAL₂, and FAL₃ were mainly affected by industrial effluent (Figure S2b). Untreated sewage effluent was raw sewage in municipal pipes, which flowed into BR owing to the overloading of wastewater treatment plants that increased the fluorescence intensity of peak FAL₂ and MHL (Figure S2c).

The FI values of sedimentary FA fractions from BR were 1.55–2.03, with an average value of 1.76 ± 0.09 (Figure S3a). Generally, FI values greater than 1.55 were associated with microbial-derived sources [34]. This shows that the biological source of sedimentary FA fractions was more significant than the terrestrial source in BR. The FI mean value in the rural section (1.85 ± 0.07) was significantly higher than those in the urban (1.74 ± 0.05) and town (1.69 ± 0.07) sections, indicating that the sedimentary FA fractions in the town and urban sections exhibited stronger aromaticity than those in the rural section.

The BIX values were positively correlated with FA fractions formed from biological activity [30]. The BIX values of sedimentary FA fractions from BR ranged from 0.67 to 1.23, with an average value of 0.93 ± 0.11 , indicating that most sediment samples of BR were dominated by FA fractions from mixed sources (Figure S3a). The rural section exhibited a higher mean BIX value (1.04 ± 0.10) than the urban (0.92 ± 0.06) and town (0.84 ± 0.09) sections. This indicates that the contribution from autochthonous sources decreased in the following order: Rural > Urban > Town.

The HIX values of sedimentary FA fractions from BR ranged from 2.14 to 9.23, with a mean value of 5.93 ± 1.91 , exhibiting a wide range of variation (Figure S3b). The town section exhibited a slightly higher mean HIX value (7.00 ± 1.75) than the urban section (6.44 ± 1.45). The rural section (4.08 ± 1.25) exhibited the lowest average value of HIX. This indicates that the sedimentary FA fractions from the town and urban sections contained higher amounts of condensed polyaromatic structures than that from the rural section. Additionally, several sediment samples from the rural section exhibited low humification levels, which may be associated with relatively low human and strong microbial activities; thus, more endogenous FA fractions were released [23]. Furthermore, all sedimentary FA fractions from the town and urban sections exhibited moderate humification levels

($4 < \text{HIX} < 10$), indicating that they were partly from exogenous input and biogeochemical processes.

3.3. Identification of PARAFAC Analysis

To characterize the composition and distribution of sedimentary FA fractions, all EEM data from the three sections were modeled using PARAFAC, and six independent components were analyzed (Figure 2 and Table S2). The six components can be grouped into two categories: one protein-like (C1) and five humus-like (C2, C3, C4, C5, and C6) components. C1 (E_x/E_m of 225 nm/380 nm) was identified as tryptophan-like (peak TRL) associated with plankton production [30]. C2 (E_x/E_m of 285 nm/390 nm) was identified as microbial humic-like (peak MHL), related to biological products from the release of algae and bacteria leachate [35]. C3 (E_x/E_m of 260 nm/470 nm) was similar to soil-derived FA-like (peak FAL₁) [36]. C4 (E_x/E_m of 240 nm/435 nm) represented the UV FA-like (peak FAL₂), which was usually derived from the breakdown of plant substances [35]. C5 (E_x/E_m of 335 nm/420 nm) was identified as visible FA-like (peak FAL₃), which was usually derived from the breakdown of animal substances [35]. The broad and long wavelength peak of C6 (E_x/E_m of 360 nm/480 nm) was categorized as terrestrial HAL compounds (peak HAL) with a high molecular weight [14].

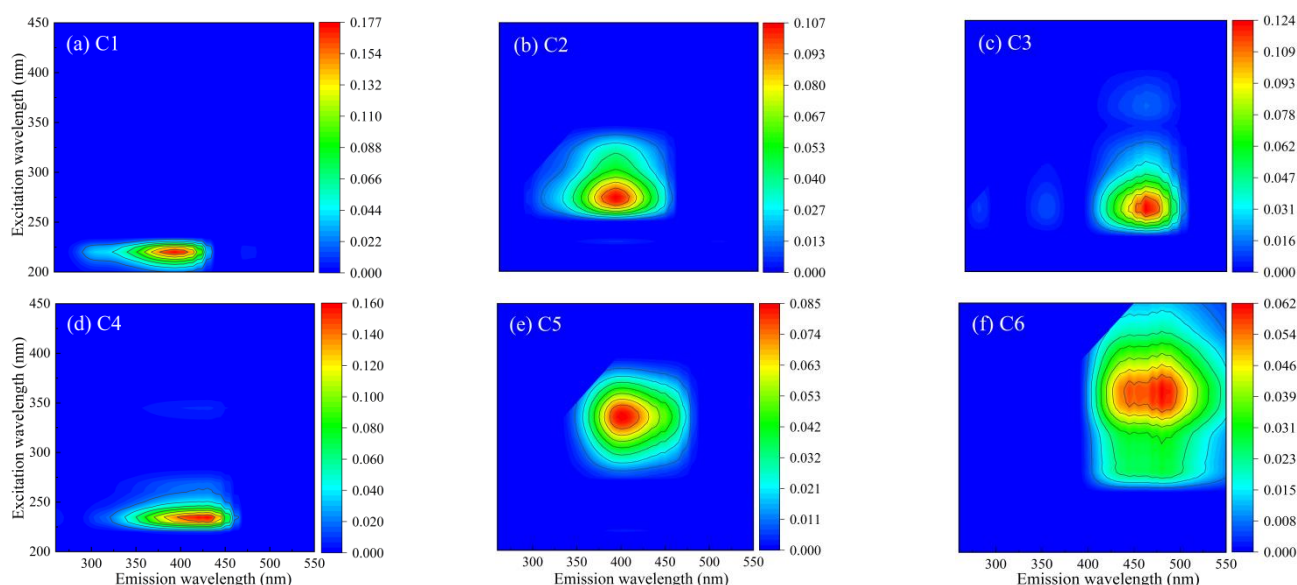


Figure 2. Six components determined by a PARAFAC model fit the EEM of sedimentary FA fractions. (a) C1; (b) C2; (c) C3; (d) C4; (e) C5; (f) C6.

3.4. Distribution in Fluorescence Components

To investigate the variations in sedimentary FA fractions from different sections, the variations in fluorescence intensity and proportion (%) of each component of the six PARAFAC components were evaluated in detail (Figure 3). The total fluorescence intensities in the town (5328.87 ± 1315.82 R.U.) and urban (4146.49 ± 535.75 R.U.) sections were significantly higher than that in the rural (2510.56 ± 611.00 R.U.) section (Figure 3a). This indicates that the town and urban sections faced heavier pollution of sedimentary FA fractions than the rural section, which may be related to the large amounts of industrial wastewater and urban domestic sewage occurring in the town and urban sections, respectively. The rural section was surrounded by sparse villages and farmlands, associated with a low intensity of anthropogenic activities, resulting in a low fluorescence intensity of sedimentary FA fractions. The proportion of each component varied owing to the different pollution source inputs (Figure 3b). For the rural section, %C4 ($26.35 \pm 1.36\%$) exhibited the highest mean value of F_{\max} proportion, followed by %C1 ($22.63 \pm 2.47\%$),

%C2 ($17.61 \pm 0.19\%$), %C3 ($16.82 \pm 2.33\%$), %C5 ($11.85 \pm 0.82\%$), and %C6 ($4.74 \pm 0.95\%$). Peak FAL₂ (C4) exhibited the strongest signal of sedimentary FA fractions in the rural section, which is likely associated with the agricultural catchments in that region [25]. Peak TRL (C1) exhibited the second-strongest signal of sedimentary FA fraction, which was a predominant biologically derived component associated with high primary production. The mean values of F_{\max} proportion in the town section decreased in the following order: %C3 ($21.05 \pm 1.34\%$) > %C4 ($19.16 \pm 3.03\%$) > %C2 ($18.79 \pm 1.18\%$) > %C5 ($17.92 \pm 3.33\%$) > %C6 ($11.98 \pm 3.14\%$) > %C1 ($11.10 \pm 4.84\%$). The mean values of F_{\max} in the urban section decreased as follows: %C4 ($23.81 \pm 0.89\%$) > %C3 ($19.85 \pm 0.94\%$) > %C1 ($18.03 \pm 1.90\%$) > %C2 ($17.67 \pm 0.75\%$) > %C5 ($13.42 \pm 0.94\%$) > %C6 ($7.22 \pm 0.75\%$). A high protein tryptophan-like (C1) abundance of sedimentary FA fractions was found in the rural and urban sections, consistent with previous studies [37,38]. The percentages of sedimentary FA fractions for the three sections decreased as follows: %C2 + %C3 + %C4 + %C5 + %C6 (humus-like, 77.37–88.90%) > %C1 (protein-like, 11.10–22.63%). As described, humus-like compounds dominated the FA fraction because the terrestrial substances were the dominant inputs, and labile protein-like compounds were rapidly consumed by microorganisms, thus contributing a lower amount of protein-like fluorescence for sedimentary FA fractions. In contrast, relatively stable humus-like compounds were preferentially preserved in the sediments under hypoxic or anoxic conditions.

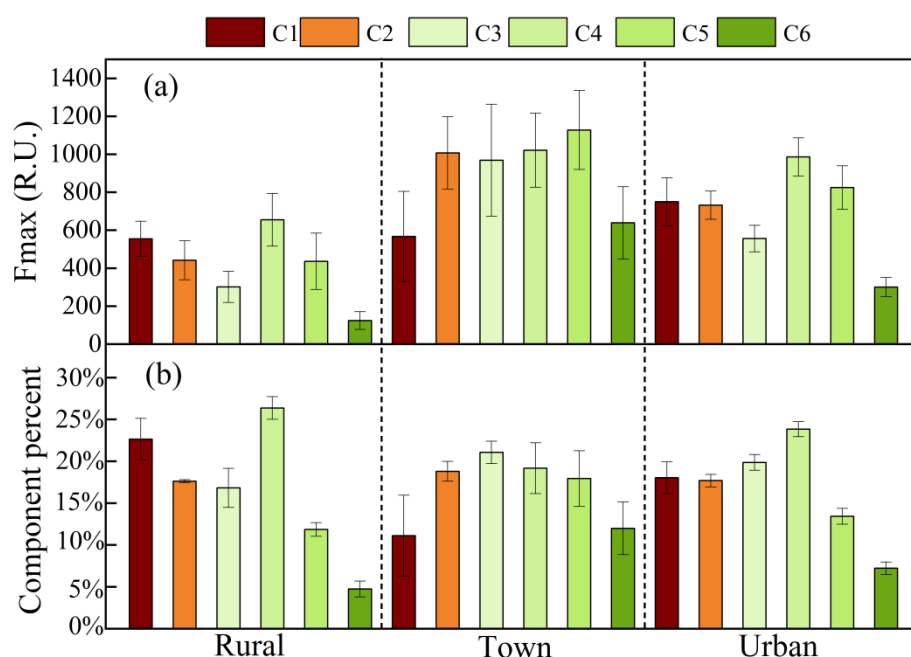


Figure 3. Plots of maximum fluorescence intensity (a) and proportion of six components (b) from the PARAFAC model in different sections.

3.5. Identification and Apportionment of Sedimentary FA Fractions Sources

The variations in sedimentary FA fractions and the influences of human activities were further investigated via PCA. Figure 4 summarizes the PCA results, including the factor loading and score plot. The loading whose absolute value was greater than 0.6 of the total variance was highlighted. The first two principal components explained 62.15% (PC1) and 23.84% (PC2) of the total variance. PC1 was positively correlated with TOC ($r = 0.868$), C2 ($r = 0.818$), C3 ($r = 0.877$), C5 ($r = 0.756$), and C6 ($r = 0.908$), but PC1 was negatively correlated with FI ($r = -0.610$). This indicates that higher PC1 was related to the terrestrial sources with condensed polyaromatic structures and humus content associated with industrial sources [29]. PC2 exhibited a strong positive correlation with TP ($r = 0.910$) and C4 ($r = 0.653$), indicating that PC2 was mainly associated with the emission of domestic sewage and agricultural effluent [39].

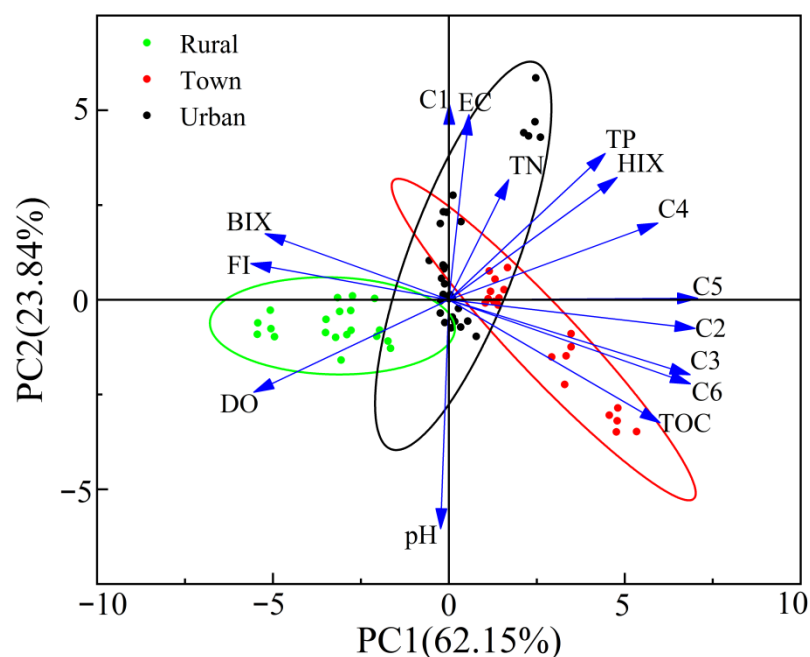


Figure 4. PCA results show the interrelation between physicochemical parameters, optical indices, and PARAFAC components. Samples are color-coded to represent the rural (green), town (red), and urban (black) groups; The green ellipse is the sedimentary FA fractions with a 95% confidence level in rural section; The red ellipse is the sedimentary FA fractions with a 95% confidence level in town section; The black ellipse is the sedimentary FA fractions with a 95% confidence level in urban section; Arrows (blue) represent the factor loadings.

The sedimentary FA fractions with a 95% confidence level formed a cluster for each ellipse in the score plot. The rural and town groups were assigned to different sides of PC1 and had different PC1 values. Sedimentary FA fraction signals of the rural group were identified by FI and BIX. In contrast, those of the town group were identified by a greater number of humus-like compounds (C2, C3, C5, and C6), which indicates a higher autochthonous feature in the rural section and a higher humification degree in the town section [40–42]. However, the urban group was located on the positive loading of PC2. It was positively correlated with C1, which may be related to the stimulated growth of phytoplankton owing to the increased nutrient level and decreased pH level in the urban section sediments. The combined results reveal that the properties of sedimentary FA fractions were affected by long-term external input, which possibly promoted autochthonous production owing to the decomposition and mineralization of terrestrial material by microbial activity and phytoplankton production.

3.6. Dynamic Variations in Sedimentary FA Fractions from Different Sections

Sedimentary FA fractions are heterogeneous and influenced by environmental factors such as pH, EC, and DO. These factors play a vital role in the dynamic variations of sedimentary FA fractions. The transformation order of the sedimentary FA fractions from different sections was further explored via 2D COS analysis.

Peak TRL was negatively correlated with FAL₁ in the synchronous and asynchronous maps (Figure 5a1,a2), while peak FAL₁ was positively correlated with FAL₂ in the two maps (Figure 5b1,b2). Moreover, peak FAL₃ was positively correlated with FAL₂ in the synchronous map but negatively correlated with FAL₂ in the asynchronous map (Figure 5c1,c2). The correlations between peak MHL and peak FAL₃ were similar to those between peak FAL₃ and peak FAL₂ (Figure 5d1,d2). According to Noda's rule [27], the sequential changes followed the order: TRL→FAL₁→FAL₂→FAL₃→MHL. Studies have shown a competitive relationship between biodegradation and photodegradation when the primary source was

endogenous [43]. Consequently, labile tryptophan-like substances in the rural section may be first transformed into relatively high concentrations of nitrogenous precursors for the formation of the FAL materials [39]. Under conditions of light radiation, microorganisms, particularly Actinobacteria, participated in the utilization of FAL components, and several complex FAL components were degraded into simple compounds, followed by the production of MHL components [44]. Particularly, the degradation order of FAL components (FAL₁, FAL₂, and FAL₃) was arranged by decreasing E_m wavelength, possibly because light destroyed and degraded the more resistant structure of FAL components into usable substrates. Peak MHL was positively correlated with peak HAL in both the synchronous and asynchronous spectra (Figure 5e1,e2), showing the order of MHL→HAL, which indicates that MAL compounds could form a stable HAL compound through microbial polymerization [45]. The sequential changes followed the order of TRL→FAL→MHL→HAL for sedimentary FA fractions in the rural section.

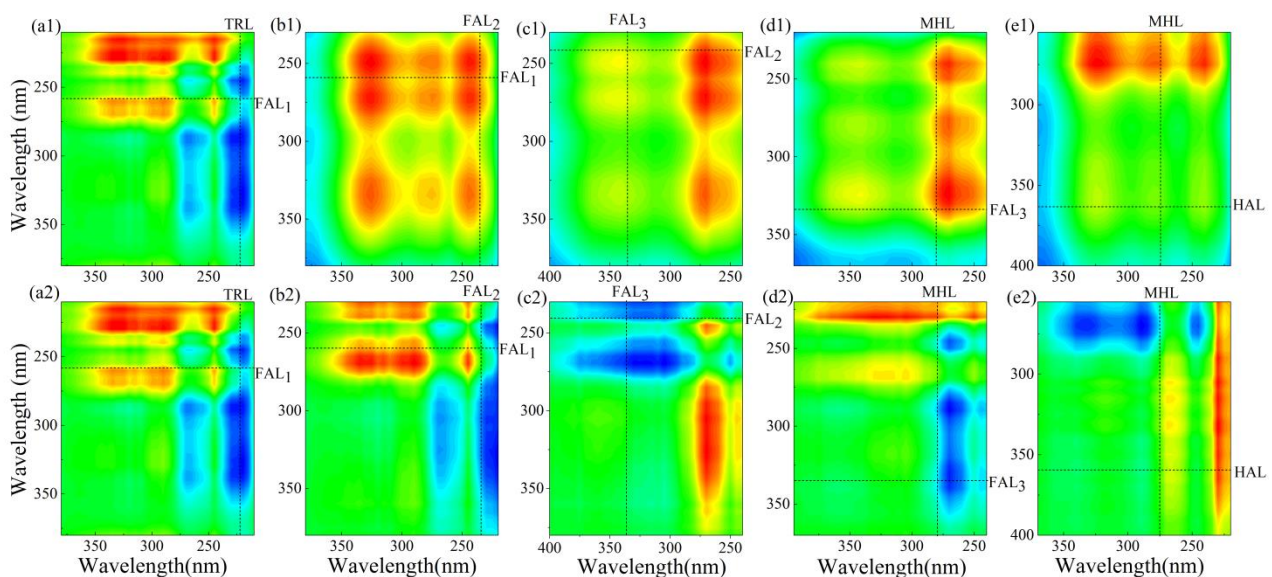


Figure 5. Synchronous and asynchronous maps from 2D-COS analysis in the rural section. Red and yellow represent positive correlations, and blue and green represent negative correlations. (a1) Synchronous map, C1 vs. C3; (a2) asynchronous map, C1 vs. C3; (b1) synchronous map, C3 vs. C4; (b2) asynchronous map, C3 vs. C4; (c1) synchronous map, C5 vs. C4; (c2) asynchronous map, C5 vs. C4; (d1) synchronous map, C2 vs. C5; (d2) asynchronous map, C2 vs. C5; (e1) synchronous map, C2 vs. C6; and (e2) asynchronous map, C2 vs. C6.

The synchronous and asynchronous maps for the town section are shown in Figure 6. Peaks TRL and FAL₂ exhibited the same relationship (Figure 6a1,a2), while peaks FAL₃ and FAL₂ exhibited opposite relationships (Figure 6b1,b2) in the two maps, indicating that the change order was TRL→FAL₂→FAL₃. The correlation between peaks FAL₃ and FAL₁ (Figure 6c1,c2) showed the same signals, while peaks MHL and FAL₁ exhibited opposite signals (Figure 6d1,d2) in the two maps, which shows that the variation order was FAL₃→FAL₁→MHL. Peaks MHL and HAL exhibited the same relationships (Figure 6e1,e2) in the two maps, indicating that the variation order was MHL→HAL. Overall, the sequence variation of sedimentary FA fractions for the town section followed the order of TRL→FAL₂→FAL₃→FAL₁→MHL→HAL, similar to the variation trend of the rural section. The variation is probably related to the same controlling factors in the rural section, such as pH (Section 3.7). However, FAL₁ degraded later than FAL₂ and FAL₃, attributable to two factors, according to the reports by Yao et al. [46]: The first is physicochemical factors (e.g., pH, DO, TN, and TP), which were the most significant contributor to the river sediment bacterial community (49.50%). The second factor is the occurrence of heavy metals, which significantly contributed to the sediment fungal community (48.00%). The highest TN con-

centration in the town section could significantly increase enzyme activity, facilitating the conversion of active lignin and cellulose and promoting the degradation process of FAL₂ derived from the breakdown of plant substances, consistent with the findings of Saiya-Cork et al. [47], who observed that N addition increased β G (cellulolytic enzyme) activity. In our previous study of heavy metals, the Naoxiao River near the town section of BR was proven to undergo heavy metal pollution, particularly by Cd and Zn [48]. The presence of heavy metals in the town section caused by exogenous input, such as through industrial sewage and domestic sewage discharge, may alter the fungal community structure and properties. For example, the heavy metals Cd and Zn can significantly affect the distribution and microbial functions of saprotrophs, which were the dominant trophic mode of the fungal community in sediment, mainly responsible for the decomposition of plant and animal residues (FAL₂ and FAL₃) [49].

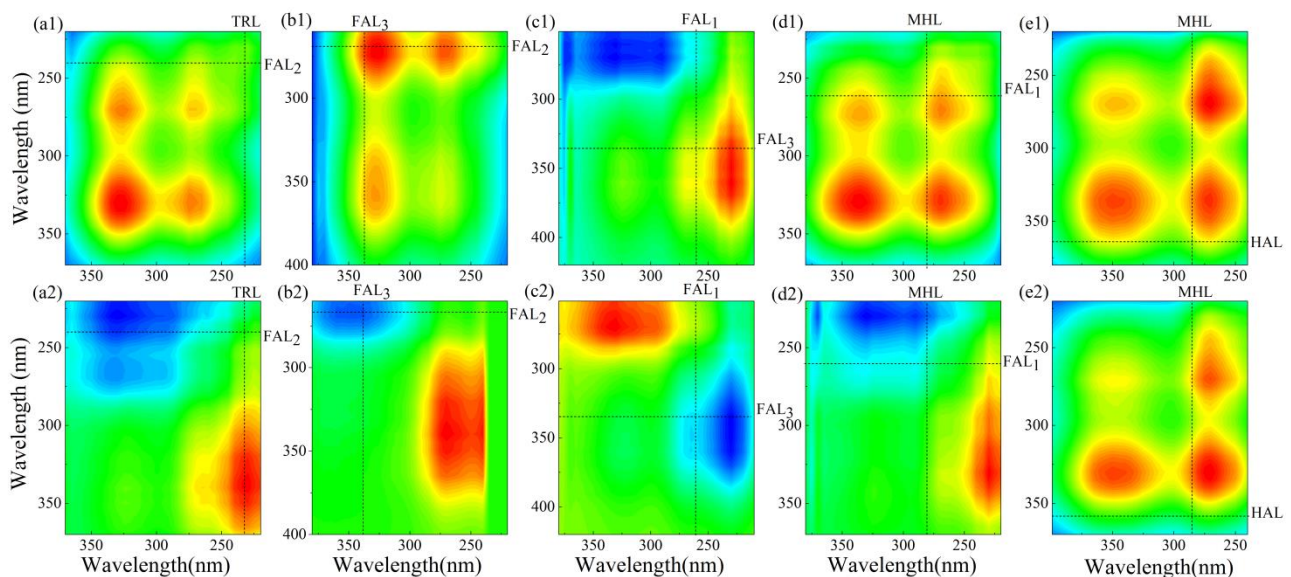


Figure 6. Synchronous and asynchronous maps from 2D-COS analysis in the town section. Red and yellow represent positive correlations, and blue and green represent negative correlations. (a1) Synchronous map, C1 vs. C4; (a2) asynchronous map, C1 vs. C4; (b1) synchronous map, C5 vs. C4; (b2) asynchronous map, C5 vs. C4; (c1) synchronous map, C5 vs. C3; (c2) asynchronous map, C5 vs. C3; (d1) synchronous map, C2 vs. C3; (d2) asynchronous map, C2 vs. C3; (e1) synchronous map, C2 vs. C6; and (e2) asynchronous map, C2 vs. C6.

Figure 7 shows the synchronous and asynchronous maps for the urban section. The relationship between peaks MHL and TRL (Figure 7a1,a2) exhibited opposite signals in the two maps. In contrast, peaks MHL and FAL₃ (Figure 7b1,b2), FAL₃ and FAL₂ (Figure 7c1,c2) and FAL₂ and FAL₁ (Figure 7d1,d2) exhibited the same signals, indicating that the variation followed the order of TRL→MHL→FAL₃→FAL₂→FAL₁. The correlation between peaks HAL and FAL₁ (Figure 7e1,e2) showed opposite signals in the two maps, indicating that the variation order was FAL₁→HAL. Hence, the sequential change order was TRL→MHL→FAL₃→FAL₂→FAL₁→HAL for the urban section, which follows increasing E_m wavelength. Generally, it has been reported that the fluorescence features at longer E_m could be linked with larger-size and higher-density structures [22]. This indicates that the formation and transformation of sedimentary FA fractions tend to be more complex and stable [50–52], consistent with the normal composting owing to the lowest DO concentration (close to anoxia state) in the urban section (Table S1). The sequential change order of sedimentary FA fractions differed among the three sections, and the effects of environmental variables and terrestrial inputs on the decomposition and polymerization of sedimentary FA fractions remain unclear. Thus, further exploring the influencing mechanism is vital.

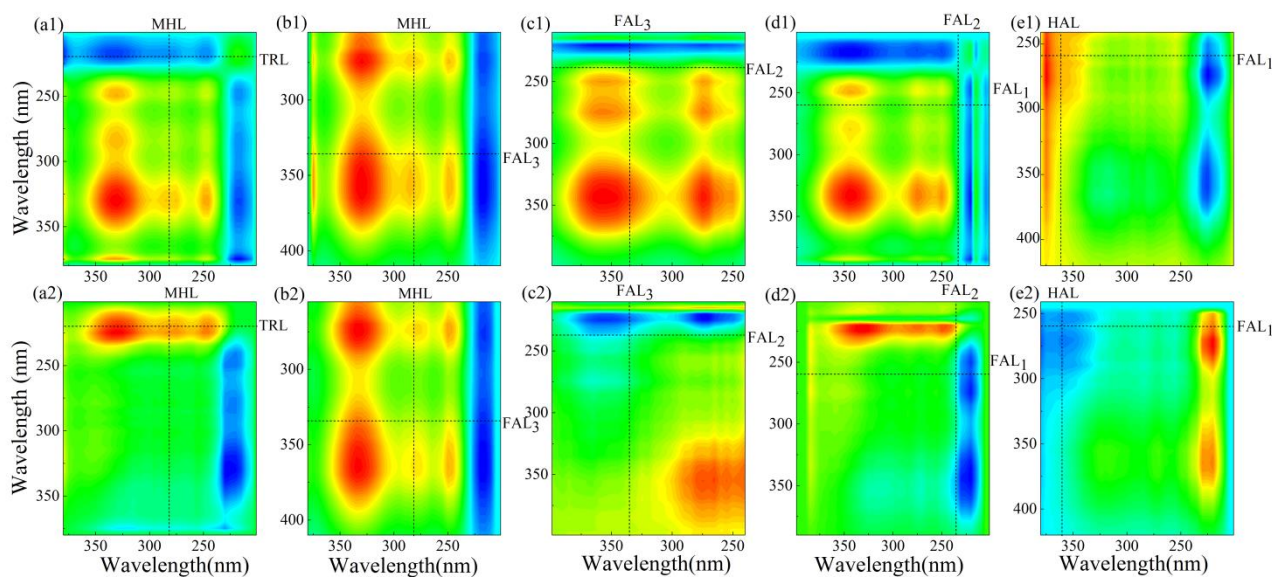


Figure 7. Synchronous and asynchronous maps from 2D-COS analysis in the urban section. Red and yellow represent positive correlations, and blue and green represent negative correlations. (a1) Synchronous map, C2 vs. C1; (a2) asynchronous map, C2 vs. C1; (b1) synchronous map, C2 vs. C5; (b2) asynchronous map, C2 vs. C5; (c1) synchronous map, C5 vs. C4; (c2) asynchronous map, C5 vs. C4; (d1) synchronous map, C4 vs. C3; (d2) asynchronous map, C4 vs. C3; (e1) synchronous map, C6 vs. C3; (e2) asynchronous map, C6 vs. C3.

3.7. Environmental Factors Affecting the Transformation of Sedimentary FA Fractions

IBM SPSS AMOS 22 was employed to further explore the causal relationships between environmental factors, nutrients, and sedimentary FA fractions from BR [53]. For Chi-square/df = 4.647 and $p = 0.000$, the SEM model revealed the correlation of environmental factors with the transformation of sedimentary FA fractions [30]. “Protein” and “Humus” were latent variables (in ovals) (Figure 8), while the others were observed variables (in rectangles). The path coefficients of TOC with pH, DO, and EC were 0.78, -0.64 , and 0.28, respectively, which may be related to the conducive effect of the environmental variables on the biological processes of sedimentary FA fractions through the influence of the variables on microbial communities and functions. Particularly, pH showed the most significant direct correlation with nutrients, which was consistent with the previous reports that pH could significantly influence the environmental behavior of the sedimentary FA fractions by altering nitrogen-related functions [4,46]. Zhang et al. [12] found that phylum Proteobacteria and Chloroflexi were the dominant phyla in the river sediment, preferring the degradation of aromatic compounds and protein-like substances. Moreover, Wang et al. [54] reported that Actinomycetes and Planctomycetes in the sediments could be potentially involved in organic matter degradation and methane and nitrogen cycling processes, and the higher abundance of Limnhabitans was related to the lower pH and its sensitivity to acid. The path coefficients of TOC with protein and humus were -0.59 and 0.65, respectively, indicating that TRL materials were mainly derived from autochthonous sources, and humic-like materials were mainly derived from allochthonous sources [21]. Moreover, protein exhibited a significant negative effect (-0.21) on the humus, and the factor loading decreased in the following order: FI (1.00) > BIX (0.98) > C1 (-0.05). Thus, FI and BIX exhibited significant indirect negative effects on humus, mediated by the latent variable of protein, particularly FI. This can be attributed to the transformation of large amounts of allochthonous FA fractions in the sediments into autochthonous FA fractions through microbial metabolism, which indicates that the autochthonous origins were dominant in BR. Additionally, the path coefficient (0.37) of TP with humus was positive, possibly because the nutrients from terrestrial input could facilitate microbial transformation or humus production [55]. All TN/TP values were <20 (Table S1), which

confirms previous reports that for TN/TP values less than 20, TN is deficient, and TP is the limiting factor [56]. TP as the prominent driver of the bacterial community, is considered closely related to chemoheterotrophy and fermentation [57]. In the humus measurement model, the factor loadings decreased in the following order: C5 (1.00) > C2 (0.99) > C3 (0.98) > C6 (0.94) > C4 (0.80). This indicates that the C5 and C2 exhibited a significant direct correlation with the latent variable of humus, related to the exogenous input and the diverse microorganisms existing in the sediment. With a higher TOC concentration and lower DO content, the bacteria in the sediment became more active, which caused a release of bacterial metabolizing FA fractions [58]. In Figure 8, doubled-headed arrows indicate correlations between variables (e.g., C1 and C2; C1 and C4), revealing that sedimentary FA fractions tended to stabilize as protein-like components were transformed into humus-like components [59], which was consistent with the results of Section 3.6.

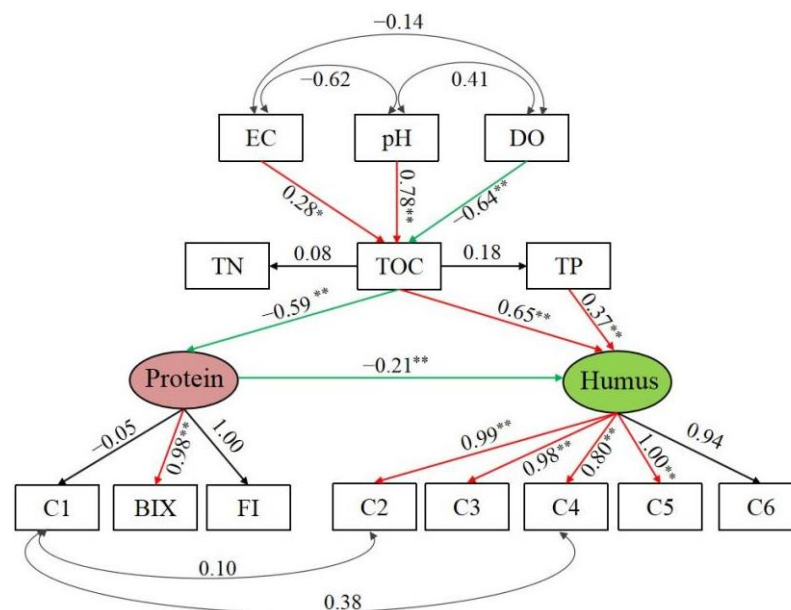


Figure 8. Predicted path model for the sedimentary FA fractions; solid red lines indicate significant positive effects, and solid green lines indicate significantly negative effects; solid black lines indicate slightly significant effects; number adjacent to the lines are the standardized coefficients; single-headed arrows represent unidirectional causal relationships; and double-headed arrows represent non-causal covariance. — Positive correlation; — Negative correlation; * $p < 0.05$; ** $p < 0.01$.

4. Conclusions

Variations in sedimentary FA fractions in three sections of an urban river were explored. In the sediments, the biological source of FA fractions was more significant than the terrestrial source, particularly in the rural section. The results of PCA revealed that the sedimentary FA fractions were mainly affected by the discharge of industrial wastewater, domestic wastewater, and agricultural effluent. Six components were identified from the sedimentary FA fractions: C1 comprised TRL compounds; C2 was associated with MHL compounds; C3, C4, and C5 were related to FAL compounds; and C6 comprised HAL compounds. The sequential variation of sedimentary FA fractions for the rural and town sections followed the order of TRL→FAL→MHL→HAL. In contrast, that of sedimentary FA fractions for the urban section followed the order of TRL→MHL→FAL→HAL. According to SEM, the pH and TP were the critical environmental variables that influenced the transformation of sedimentary FA fractions, labile protein-like component (C1) was transformed into a stable HAL component (C6), and the stable HAL component might persist for a long time in the environment and promote the internal release. Consequently, the strict control of external source discharge and the adoption of remedial measures to improve the river ecosystem is highly recommended.

Supplementary Materials: The following supporting information can be downloaded at: <https://www.mdpi.com/article/10.3390/w15122256/s1>, Table S1: Physicochemical properties of sediments, overlying bottom water, and sedimentary FA fractions from BR, China; Table S2. Description of the six PARAFAC model components from the sedimentary FA fractions; Figure S1: Boxplots display the spatial variation of physicochemical parameters. White circles indicate the mean values, boxes show standard error, and whiskers delimit maximum and minimum; Figure S2: Representative EEM of sedimentary FA fractions with various pollution types and sources: (a) agricultural effluent (S1); (b) industrial effluent (S8); and (c) untreated sewage effluent (S13); Figure S3: Spatial variations of the values of FI, BIX and HIX.

Author Contributions: Y.X.: Methodology, Software, Data curation, and Writing—original draft. H.Y.: Investigation, Resources, Writing—review & editing, and Data curation. Y.S.: Writing—review & editing and Supervision. All authors have read and agreed to the published version of the manuscript.

Funding: This work was supported by the National Key R&D Program of China (No. 2021YFC3201500), the Natural Science Foundation of Fujian Province (Nos. 2020J011374 and 2021J01500), the Fujian Provincial Department of Science and Technology (Nos. 2020R1032002 and 2020R1032006), and the Foreign Cooperation Project of Fujian Academy of Agricultural Sciences (No. DWHZ-2022-17).

Institutional Review Board Statement: Not applicable.

Informed Consent Statement: Not applicable.

Data Availability Statement: Not applicable.

Acknowledgments: The authors are grateful to the editors and the anonymous reviewers for their insightful comments and suggestions.

Conflicts of Interest: The authors declare no conflict of interest.

References

1. Nargis, A.; Habib, A.; Harun, O.R.; Harun, H.B.; Islam Sarker, M.S.; Jin, R.; Cai, M. Status of multielement in water of the river Buriganga, Bangladesh: Aquatic chemistry of metal ions in polluted river water. *Emerg. Contam.* **2021**, *7*, 99–115. [[CrossRef](#)]
2. Ali, J.; Li, Y.; Wang, X.J.; Zhao, J.; Xi, N.N.; Zhang, Z.R.; Xia, X.H. Climate-zone-dependent effect mechanism of humic acid and fulvic acid extracted from riverine sediments on aggregation behavior of graphene oxide. *Sci. Total Environ.* **2020**, *721*, 137682. [[CrossRef](#)] [[PubMed](#)]
3. Gontijo, E.S.J.; Herzsprung, P.; Lechtenfeld, O.J.; de CBueno, C.; ACBarth, J.; Rosa, A.H.; Friese, K. Multi-proxy approach involving ultrahigh resolution mass spectrometry and self-organising maps to investigate the origin and quality of sedimentary organic matter across a subtropical reservoir. *Org. Geochem.* **2021**, *151*, 104165. [[CrossRef](#)]
4. Song, F.H.; Wu, F.C.; Guo, F.; Wang, H.; Feng, W.Y.; Zhou, M.; Deng, Y.H.; Bai, Y.C.; Xing, B.S.; Giesy, J.P. Interactions between stepwise-eluted sub-fractions of fulvic acids and protons revealed by fluorescence titration combined with EEM-PARAFAC. *Sci. Total Environ.* **2017**, *605–606*, 58–65. [[CrossRef](#)] [[PubMed](#)]
5. Fallah, R.E.; Rouillon, R.; Vouvé, F. Spectral characterization of the fluorescent components present in humic substances, fulvic acid and humic acid mixed with pure benzo (a) pyrene solution. *Spectrochim. Acta Part A Mol. Biomol. Spectrosc.* **2018**, *199*, 71–79. [[CrossRef](#)]
6. Qian, G.R.; Xu, L.; Li, N.; Wang, K.L.; Qu, Y.W.; Xu, Y.F. Enhanced arsenic migration in tailings soil with the addition of humic acid, fulvic acid and thiol-modified humic acid. *Chemosphere* **2022**, *286*, 131784. [[CrossRef](#)]
7. Cui, H.Y.; Wen, X.; Wu, Z.H.; Zhao, Y.; Lu, Q.; Wei, Z. Insight into complexation of Cd(II) and Cu(II) to fulvic acid based on feature recognition of PARAFAC combined with 2DCOS. *J. Hazard. Mater.* **2022**, *440*, 129758. [[CrossRef](#)]
8. Li, H.; Wang, J.H.; Zhao, B.Y.; Gao, M.S.; Shi, W.J.; Zhou, H.J.; Xie, Z.L.; Zhou, B.; Lü, C.W.; He, J. The role of major functional groups: Multi-evidence from the binding experiments of heavy metals on natural fulvic acids extracted from lake sediments. *Ecotoxicol. Environ. Saf.* **2018**, *162*, 514–520. [[CrossRef](#)]
9. Yu, H.B.; Song, Y.H.; Du, E.; Yang, N.; Peng, J.F.; Liu, R.X. Comparison of PARAFAC components of fluorescent dissolved and particular organic matter from two urbanized rivers. *Environ. Sci. Pollut. Res.* **2016**, *23*, 10644–10655. [[CrossRef](#)]
10. Aranganathan, L.; Radhika Rajasree, S.R.; Govindaraju, K.; Sivarathna kumar, S.; Gayathri, S.; Remya, R.R.; Suman, T.Y. Spectral and microscopic analysis of fulvic acids isolated from marine fish waste and sugarcane bagasse co-compost. *Biocatal. Agric. Biotechnol.* **2020**, *29*, 101762. [[CrossRef](#)]
11. Wen, Z.D.; Song, K.S.; Shang, Y.X.; Lyu, L.L.; Tao, H.; Liu, G. Natural and anthropogenic impacts on the DOC characteristics in the Yellow River continuum. *Environ. Pollut.* **2021**, *287*, 117231. [[CrossRef](#)] [[PubMed](#)]
12. Zhang, L.; Sun, Q.X.; Dou, Q.H.; Lan, S.; Peng, Y.Z.; Yang, J.C. The molecular characteristics of dissolved organic matter in urbanized riverine sediments and their environmental impact under the action of microorganisms. *Sci. Total Environ.* **2022**, *827*, 154289. [[CrossRef](#)] [[PubMed](#)]

13. Feng, L.K.; Zhang, J.; Fan, J.L.; Wei, L.L.; He, S.F.; Wu, H.M. Tracing dissolved organic matter in inflowing rivers of Nansi Lake as a storage reservoir: Implications for water-quality control. *Chemosphere* **2021**, *286*, 131624. [[CrossRef](#)] [[PubMed](#)]
14. Xu, X.T.; Kang, J.; Shen, J.M.; Zhao, S.X.; Wang, B.Y.; Zhang, X.X.; Chen, Z.L. EEM-PARAFAC characterization of dissolved organic matter and its relationship with disinfection by-products formation potential in drinking water sources of northeastern China. *Sci. Total Environ.* **2021**, *774*, 145297. [[CrossRef](#)] [[PubMed](#)]
15. Fan, T.T.; Yao, X.; Ren, H.Y.; Liu, L.; Deng, H.G.; Shao, K.Q. Regional-scale investigation of the molecular weight distribution and metal-binding behavior of dissolved organic matter from a shallow macrophytic lake using multispectral techniques. *J. Hazard. Mater.* **2022**, *439*, 129532. [[CrossRef](#)]
16. Lupi, L.; Bertrand, L.; Monferrán, M.V.; Amé, M.V.; Diaz, M.P. Multilevel and structural equation modeling approach to identify spatiotemporal patterns and source characterization of metals and metalloids in surface water and sediment of the Ctalamochita River in Pampa region, Argentina. *J. Hydrol.* **2019**, *572*, 403–413. [[CrossRef](#)]
17. Liu, D.P.; Lu, K.T.; Yu, H.B.; Gao, H.J.; Xu, W.N. Applying synchronous fluorescence spectroscopy conjunct second derivative and two-dimensional correlation to analyze the interactions of copper (II) with dissolved organic matter from an urbanized river. *Talanta* **2021**, *235*, 122738. [[CrossRef](#)]
18. Soon, Y.K.; Kalra, Y.P. Short communication: A comparison of plant tissue digestion methods for nitrogen and phosphorus analyses. *Can. J. Soil Sci.* **1995**, *75*, 243–245. [[CrossRef](#)]
19. Bao, S. *Soil Agrochemical Analysis*; China Agricultural Press: Beijing, China, 2000; Volume 30.
20. Guo, X.; Yu, H.; Yan, Z.; Gao, H.; Zhang, Y. Tracking variations of fluorescent dissolved organic matter during wastewater treatment by accumulative fluorescence emission spectroscopy combined with principal component, second derivative and canonical correlation analyses. *Chemosphere* **2018**, *194*, 463–470. [[CrossRef](#)]
21. Liu, D.P.; Yu, H.B.; Gao, H.J.; Liu, X.Y.; Xu, W.N.; Yang, F. Insight into structural composition of dissolved organic matter in saline alkali soil by fluorescence spectroscopy coupled with self-organizing map and structural equation modeling. *Spectrochim. Acta Part A Mol. Biomol. Spectrosc.* **2022**, *279*, 121311. [[CrossRef](#)]
22. Aftab, B.; Shin, H.S.; Hur, J. Exploring the fate and oxidation behaviors of different organic constituents in landfill leachate upon Fenton oxidation processes using EEM-PARAFAC and 2D-COS-FTIR. *J. Hazard. Mater.* **2018**, *354*, 33–41. [[CrossRef](#)]
23. Zhang, H.; Cui, K.P.; Guo, Z.; Li, X.Y.; Chen, J.; Qi, Z.G.; Xu, S.Y. Spatiotemporal variations of spectral characteristics of dissolved organic matter in river flowing into a key drinking water source in China. *Sci. Total Environ.* **2020**, *700*, 10. [[CrossRef](#)] [[PubMed](#)]
24. Niloy, N.M.; Haque, M.M.; Tareq, S.M. Characterization of dissolved organic matter at urban and industrial rainwater of Bangladesh by fluorescence spectroscopy and EEM-PARAFAC modeling. *Environ. Chall.* **2021**, *5*, 100250. [[CrossRef](#)]
25. Duplá, M.V. Characterization of cDOM in the Elkhorn Slough estuary using EEM spectroscopy and its potential for macrophyte monitoring. *J. Mar. Syst.* **2022**, *226*, 103661. [[CrossRef](#)]
26. Wu, J.Q.; Yao, W.K.; Zhao, L.; Zhao, Y.; Qi, H.S.; Zhang, R.J.; Song, C.H.; Wei, Z.M. Estimating the synergistic formation of humus by abiotic and biotic pathways during composting. *J. Clean. Prod.* **2022**, *363*, 132470. [[CrossRef](#)]
27. Noda, I. Generalized two-dimensional correlation method applicable to infrared, raman, and other types of spectroscopy. *Appl. Spectrosc.* **1993**, *47*, 1329–1336. [[CrossRef](#)]
28. Maqbool, T.; Hur, J. Changes in fluorescent dissolved organic matter upon interaction with anionic surfactant as revealed by EEM-PARAFAC and two-dimensional correlation spectroscopy. *Chemosphere* **2016**, *161*, 190–199. [[CrossRef](#)] [[PubMed](#)]
29. Shafiquzzaman, M.; Ahmed, A.T.; Shafiul Azam, M.; Razzak, A.; Askri, B.; Hassan, H.F.; Ravikumar, B.N.; Okuda, T. Identification and characterization of dissolved organic matter sources in Kushiro river impacted by a wetland. *Ecol. Eng.* **2014**, *70*, 459–464. [[CrossRef](#)]
30. Lu, K.T.; Gao, H.J.; Yu, H.B.; Liu, D.P.; Zhu, N.M.; Wan, K.L. Insight into variations of DOM fractions in different latitudinal rural black-odor waterbodies of eastern China using fluorescence spectroscopy coupled with structure equation model. *Sci. Total Environ.* **2022**, *816*, 151531. [[CrossRef](#)]
31. Hooper, D.; Coughlan, J.; Mullen, M.R. Structural equation modelling: Guidelines for determining model fit. *Electron. J. Bus. Res. Methods* **2008**, *6*, 53–60.
32. Mahabeer, P.; Tekere, M. Anthropogenic pollution influences on the physical and chemical quality of water and sediments of the umdloti river system, Kwazulu-Natal. *Phys. Chem. Earth* **2021**, *123*, 103030. [[CrossRef](#)]
33. Chakraborty, P.; Chakraborty, S.; Jayachandran, S.; Madan, R.; Sarkar, A.; Linsy, P.; Nath, B.N. Effects of bottom water dissolved oxygen variability on copper and lead fractionation in the sediments across the oxygen minimum zone, western continental margin of India. *Sci. Total Environ.* **2016**, *556*, 1052–1061. [[CrossRef](#)] [[PubMed](#)]
34. Cory, R.M.; Miller, M.P.; McKnight, D.M.; Guerard, J.J.; Miller, P.L. Effect of instrument-specific response on the analysis of fulvic acid fluorescence spectra. *Limnol. Oceanogr. Methods* **2010**, *8*, 67–78.
35. Pitta, E.; Zeri, C. The impact of combining data sets of fluorescence excitation–emission matrices of dissolved organic matter from various aquatic sources on the information retrieved by PARAFAC modeling. *Spectrochim. Acta Part A Mol. Biomol. Spectrosc.* **2021**, *258*, 119800. [[CrossRef](#)]
36. Osburn, C.L.; Boyd, T.J.; Montgomery, M.T.; Bianchi, T.S.; Coffin, R.B.; Paerl, H.W. Optical proxies for terrestrial dissolved organic matter in estuaries and coastal waters. *Front. Mar. Sci.* **2016**, *2*, 127. [[CrossRef](#)]
37. Ma, Y.M.; Mao, R.; Li, S.Y. Hydrological seasonality largely contributes to riverine dissolved organic matter chemical composition: Insights from EEM-PARAFAC and optical indicators. *J. Hydrol.* **2021**, *595*, 125993. [[CrossRef](#)]

38. Wilson, H.F.; Xenopoulos, M.A. Effects of agricultural land use on the composition of fluvial dissolved organic matter. *Nat. Geosci.* **2009**, *2*, 37–41. [[CrossRef](#)]
39. Yu, Z.; Liu, X.M.; Zhao, M.H.; Zhao, W.Q.; Liu, J.; Tang, J.; Liao, H.P.; Chen, Z.; Zhou, S.G. Hyperthermophilic composting accelerates the humification process of sewage sludge: Molecular characterization of dissolved organic matter using EEM-PARAFAC and two-dimensional correlation spectroscopy. *Bioresour. Technol.* **2019**, *274*, 198–206. [[CrossRef](#)]
40. Asaoka, S.; Jadoon, W.A.; Umehara, A.; Takeda, K.; Otani, S.; Ohno, M.; Fujitake, N.; Sakugawa, H.; Okamura, H. Organic matter degradation characteristics of coastal marine sediments collected from the Seto Inland Sea, Japan. *Mar. Chem.* **2020**, *225*, 103854. [[CrossRef](#)]
41. Shen, D.L.; Huang, S.H.; Zhang, Y.P.; Zhou, Y.C. The source apportionment of N and P pollution in the surface waters of lowland urban area based on EEM-PARAFAC and PCA-APCS-MLR. *Environ. Res.* **2021**, *197*, 111022. [[CrossRef](#)]
42. Zhou, Y.Q.; Zhang, Y.L.; Jeppesen, E.; Murphy, K.R.; Shi, K.; Liu, M.L.; Liu, X.H.; Zhu, G.W. Inflow rate-driven changes in the composition and dynamics of chromophoric dissolved organic matter in a large drinking water lake. *Water Res.* **2016**, *100*, 211–221. [[CrossRef](#)] [[PubMed](#)]
43. Tranvik, L.J.; Bertilsson, S. Contrasting effects of solar UV radiation on dissolved organic sources for bacterial growth. *Ecol. Lett.* **2008**, *4*, 458–463. [[CrossRef](#)]
44. Song, X.Y.; Zhao, M.Y.; Chen, A.Q.; Xie, X.Y.; Yang, H.Y.; Zhang, S.B.; Wei, Z.M.; Zhao, Y. Effects of input of terrestrial materials on photodegradation and biodegradation of DOM in rivers: The case of Heilongjiang River. *J. Hydrol.* **2022**, *609*, 127792. [[CrossRef](#)]
45. Zhang, J.; Lv, B.Y.; Xing, M.Y.; Yang, J. Tracking the composition and transformation of humic and fulvic acids during vermicomposting of sewage sludge by elemental analysis and fluorescence excitation-emission matrix. *Waste Manag.* **2015**, *39*, 111–118. [[CrossRef](#)] [[PubMed](#)]
46. Yao, Y.; Zhao, J.Q.; Miao, L.Z.; Hou, J. Effects of sediment physicochemical factors and heavy metals on the diversity, structure, and functions of bacterial and fungal communities from a eutrophic river. *Environ. Pollut.* **2022**, *303*, 119129. [[CrossRef](#)]
47. Saiya-Cork, K.R.; Sinsabaugh, R.L.; Zak, D.R. The effects of long-term nitrogen deposition on extracellular enzyme activity in an *Acer saccharum* forest soil. *Soil Biol. Biochem.* **2002**, *34*, 1309–1315. [[CrossRef](#)]
48. Xiao, Y.C.; Yu, H.B.; Song, Y.H. Spatial differentiation characteristics and response relationship of DOM, nutrients, and heavy metals in river sediments. *Environ. Sci.* **2022**, *43*, 226–236. [[CrossRef](#)]
49. Wang, J.; Yuan, S.; Tang, L.; Pan, X.; Pu, X.; Li, R.; Shen, C. Contribution of heavy metal in driving microbial distribution in a eutrophic river. *Sci. Total Environ.* **2020**, *712*, 136295. [[CrossRef](#)]
50. Bai, Y.C.; Wu, F.C.; Xing, B.S.; Meng, W.; Shi, G.L.; Ma, Y.; Giesy, J.P. Isolation and characterization of Chinese standard fulvic acid sub-fractions separated from forest soil by stepwise elution with pyrophosphate buffer. *Sci. Rep.* **2015**, *5*, 8723. [[CrossRef](#)]
51. Carvalho, S.I.; Otero, M.; Duarte, A.C.; Santos, E.B. Spectroscopic changes on fulvic acids from a kraft pulp mill effluent caused by sun irradiation. *Chemosphere* **2008**, *73*, 1845–1852. [[CrossRef](#)]
52. Łomińska-Płatek, D.; Anielak, A.M. Quantitative balance and analysis of fulvic acids changes in the process of municipal sewage treatment. *Water Resour. Ind.* **2021**, *26*, 100155. [[CrossRef](#)]
53. Igolkina, A.A.; Meshcheryakov, G. semopy: A python package for structural equation modeling. *Struct. Equ. Model. Multidiscip. J.* **2020**, *27*, 952–963. [[CrossRef](#)]
54. Wang, H.J.; Liu, X.C.; Wang, Y.L.; Zhang, S.Q.; Zhang, G.M.; Han, Y.Y.; Li, M.X.; Liu, L. Spatial and temporal dynamics of microbial community composition and factors influencing the surface water and sediments of urban rivers. *J. Environ. Sci.* **2023**, *124*, 187–197. [[CrossRef](#)]
55. Williams, C.J.; Yamashita, Y.; Wilson, H.F.; Jaffé, R.; Xenopoulos, M.A. Unraveling the role of land use and microbial activity in shaping dissolved organic matter characteristics in stream ecosystems. *Limnol. Oceanogr.* **2010**, *55*, 1159–1171. [[CrossRef](#)]
56. Guildford, S.J.; Hecky, R.E. Total nitrogen, total phosphorus, and nutrient limitation in lakes and oceans: Is there a common relationship. *Limnol. Oceanogr.* **2000**, *45*, 1213–1223. [[CrossRef](#)]
57. Jiao, C.; Zhao, D.; Zeng, J.; Guo, L.; Yu, Z. Disentangling the seasonal co-occurrence patterns and ecological stochasticity of planktonic and benthic bacterial communities within multiple lakes. *Sci. Total Environ.* **2020**, *740*, 140010. [[CrossRef](#)]
58. Cao, J.X.; Sun, Q.; Zhao, D.H.; Xu, M.Y.; Shen, Q.S.; Wang, D.; Wang, Y.; Ding, S.M. A critical review of the appearance of black-odorous waterbodies in China and treatment methods. *J. Hazard. Mater.* **2020**, *385*, 18. [[CrossRef](#)]
59. Zhu, L.J.; Zhao, Y.; Bai, S.C.; Zhou, H.X.; Chen, X.M.; Wei, Z.M. New insights into the variation of dissolved organic matter components in different latitudinal lakes of northeast China. *Limnol. Oceanogr.* **2020**, *65*, 471–481. [[CrossRef](#)]

Disclaimer/Publisher's Note: The statements, opinions and data contained in all publications are solely those of the individual author(s) and contributor(s) and not of MDPI and/or the editor(s). MDPI and/or the editor(s) disclaim responsibility for any injury to people or property resulting from any ideas, methods, instructions or products referred to in the content.